# Plastic deformation processes in Cu/Sn bimetallic films

K.S. Kumar,[a] L. Reinbold,[b] A.F. Bower, and E. Chason
*Division of Engineering, Brown University, Providence, Rhode Island 02912*

(Received 13 April 2008; accepted 18 July 2008)

Although the driving force for the growth of Sn whiskers from the surface of Sn coatings on copper is thought to be internally generated stress due to the formation of $Cu_6Sn_5$ at the Cu/Sn interface, little is known about the nature of this internal stress and how it cracks the surface Sn oxide (an important precursor to whisker formation). Arguments based on elasticity alone do not appear to be sufficient and suggest an important role for plastic deformation. Direct observations, made by transmission electron microscopy of cross-sectioned bimetallic Cu/Sn thin-film specimens, confirm plastic deformation of the Sn grains due to the formation of $Cu_6Sn_5$. Dislocation motion and pile-up at the surface Sn oxide, rotation associated with subgrain boundary formation, interaction of the subgrain boundaries with the Sn surface, and diffusional processes are various mechanisms that can produce stress at the Sn surface and crack the Sn oxide.

## I. INTRODUCTION

The formation of single-crystal whiskers on the surface of metals such as Sn, Zn, Cd, and Al has been studied over the past six decades,[1–6] and in the 1950s, significant effort was expended in understanding the mechanism of whisker growth.[7–10] The particular case of the formation of whiskers from the Sn surface when it is electroplated on copper has been of significant interest to the microelectronics industry.[2,11–15] Such Sn whiskers are usually a couple of micrometers in diameter but can grow to several millimeters in length over time while an electronic component is in service. These whiskers can bridge the gaps between closely spaced interconnects and can create short circuits, leading to system failure. Numerous examples of such failures have been documented in the literature and include pacemakers, satellites, and missiles.[13,16–20] The problem of Sn whiskering had been circumvented by adding Pb to Sn, but recent international regulations that require the elimination of Pb from electronic components have led to a re-emergence of significant scientific and technological interest and a flurry of research activity in this area.[11,14,15,21]

Various driving forces have been suggested for whisker formation, including recrystallization,[1,22–25] oxidation,[7,8,26] and stress in the layers.[5,11,12,21,27–40] Fisher et al.[33] in 1954 first demonstrated that compressive stress in the Sn layer can serve as a driving force for whisker growth by applying ring clamps to Sn-plated steel specimens and measuring whisker growth rates as a function of clamping pressure and time. The current consensus is that stress (externally applied or internally generated) is the primary driving force for whisker formation, but there is still significant disagreement about how and where the stress is generated and how it leads to whisker formation. Stress may arise from different internal sources, including: (i) residual stresses that develop during the deposition process, (ii) diffusion of Cu into Sn, (iii) the formation of an intermetallic compound between the Cu and Sn, and (iv) thermal-expansion–mismatch stresses that may develop under thermal cycling conditions.

The internal stresses that develop in the Sn and Cu layers have been measured in several investigations. Lindborg[5,6] presented the first measurement of internal stresses made by a cantilever beam method on Zn films plated over steel substrates. More recently, Lee and Lee[11] have measured stress in Sn layers on Cu using a beam deflection method. They proposed that a compressive stress of 8–10 MPa in the Sn layer develops as a consequence of the formation of $Cu_6Sn_5$ particles at/along Sn grain boundaries near the Cu/Sn interface. They postulated that the resulting elastic biaxial stress gives rise to elastic strains normal to the film plane, with the magnitude of the strain being dependent on the grain orientation as a consequence of the anisotropic character of the elastic

[a] Address all correspondence to this author.
e-mail: Sharvan_Kumar@brown.edu
This author was an editor of this journal during the review and decision stage. For the *JMR* policy on review and publication of manuscripts authored by editors, please refer to http://www.mrs.org/jmr_policy
[b] Present address: Raytheon Company IDS, Maritime Mission Center, Portsmouth, RI 02871.
DOI: 10.1557/JMR.2008.0351

 

modulus. The consequential shear strains at the grain boundary were claimed to cause the cracking of the surface Sn oxide film, and this allowed the Sn to extrude from the grains whose surface oxide film was sheared. Zhang et al.[38,39] used a flexure beam technique to make in situ measurements of stress in bright and satin-bright Sn coatings and reported compressive stress values in the Sn. They supported the observations of Lee and Lee, namely, that $Cu_6Sn_5$ particles grow into the Sn grain boundaries. Further studies using x-ray measurements correlated the development of stress in Cu/Sn films with whisker formation.[28]

Tu and co-workers used x-ray diffraction (XRD)[12] and Rutherford backscattering spectroscopy (RBS)[13] to study the kinetics of intermetallic compound formation in vapor-deposited Cu/Sn films and concluded that Cu is the dominant diffusing species, that Cu diffusion is interstitial in Sn, and that the intermetallic growth rate is limited by reaction at the interface of the growing particle. Further work[14] suggested that whisker growth occurred by long-range diffusion of Sn atoms to relieve compressive stress due to the formation of the intermetallic and led to an analytical model relating whisker growth kinetics to the Sn stress.

Choi et al.[30] utilized microdiffractometry via synchrotron radiation to characterize stress states in the region around a whisker root. It was observed that the stress is highly inhomogeneous and varies from grain to grain (the stress is biaxial only when averaged over several grains). The stress gradient from the whisker root to the surrounding area was taken to indicate that the growth of the whisker relieves most of the local compressive stress. Boettinger et al.[21] used beam deflection to compare stress evolution and whisker formation on Sn/Cu and Sn(Pb)/Cu electrodeposited layers. Their results point to the importance of the layer composition in affecting the growth of the intermetallic particles and altering the stress state. This work included careful characterization of the different microstructures associated with the different layer compositions. To explain the measured stresses, Galyon and Palmer[40] recently proposed a zonal model that includes the effects of vacancy formation in the Cu layer and volumetric expansion in the IMC layer to create regions of different stresses in the Sn–Cu structure.

Much of the previous analytical work discussed above has focused primarily on elastic stresses generated by the volumetric expansion of the IMC particles as they grow into the overlying Sn layer. However, elastic stress typically decreases rapidly away from a growing particle (on the order of $1/r^3$, where $r$ is the distance from the particle[41]), whereas plastic relaxation processes produce dislocations that can glide until they reach a barrier such as a grain boundary/hard surface and pile up (provided adequate stress is available to keep them moving); a pile-up stress can then act on the barrier far away from the source of the dislocations. Furthermore, at room temperature, Sn is at a significant fraction of its melting point (~$0.6T_m$) and has a low yield stress, so that diffusion-dependent processes such as creep (Nabarro–Herring and Coble creep) and dislocation glide and climb (dynamic recovery) will participate in accommodating mismatch strains.

Despite their likely importance, these mechanisms have not been given adequate consideration in the literature. To address these issues, we have performed studies to examine stress evolution in Sn in Cu/Sn bimetal films as a function of time and coupled them with detailed TEM analysis of cross sections of Cu/Sn bimetal films that had been allowed to react for various lengths of time. This has enabled an understanding of microstructural evolution with time and identification of the underlying deformation mechanisms that may be responsible for the observed stress evolution. The possible role of plastic deformation of Sn in cracking the Sn oxide and enabling Sn whisker formation is discussed.

## II. EXPERIMENTAL

A batch of bilayer Cu/Sn films was grown at the same time by electron-beam evaporation of Cu and Sn layers onto oxidized Si wafers; this enabled high purity of the components to be maintained in each layer. Prior to metal deposition, the 375-μm-thick silicon wafer substrates (25.4 mm × 12.5 mm rectangles, with a 100-nm-thick $SiO_2$ layer) were cleaned using a standard industry cleaning procedure described as follows: 5 min in an acetone bath (ultrasonic agitation), 5 min in a methanol bath (ultrasonic agitation), 5 min in a de-ionized (DI) water rinse, followed by drying with compressed nitrogen. The physical vapor-deposited (PVD) samples were made by consecutive evaporation of 1200-nm Sn on 600-nm Cu (at a deposition rate of 0.5 nm/s) on the silicon wafers in a Temescal electron-beam evaporator, under a vacuum of $1.33 \times 10^{-4}$ Pa. A 10-nm layer of titanium was deposited first to enhance adhesion of the copper layer to the silicon wafer substrate. For comparison, a similar set of specimens was also produced by electrodeposition of Sn (using a commercial plating solution) on vapor-deposited Cu. Both deposition techniques produced a columnar microstructure with a surface roughness that was comparable for films of equal thickness. We mention the electrodeposited samples because brighteners are often used in industrial electroplating processes that produce grain refinement and reduced surface roughness. Such differences in surface morphology and microstructure may modify the stress evolution as well as the whisker growth kinetics. However, without the use of additives, similar microstructures to vapor-deposited samples can be obtained. The electrodeposited samples are not discussed further in this paper.

The samples were characterized after different time intervals to determine the kinetics. The stress evolution was measured using a wafer curvature technique that utilizes a multibeam optical stress sensor (MOSS).[42,43] Stress in the film induces bending in the wafer which changes the spacing of the array of parallel laser beams and is measured with a CCD camera. As described by the Stoney formula, the stress is directly proportional to the measured curvature, $\kappa$:

$$\kappa = \frac{6\sigma h_f}{M_s h_s^2} \quad ,$$

where $\sigma$ is the average film stress, $h_f$ and $h_s$ are the film and substrate thicknesses, and $M_s$ is the biaxial modulus of the substrate. For multilayer systems, $\sigma h_f$ is replaced by a sum over the average stress and thickness of each layer:

$$\kappa = \frac{6}{M_s h_s^2} \sum \sigma_i h_i \quad .$$

Thus, the curvature is related to a product of the film stress and layer thickness for the composite structure.

To determine the stress in the Sn layer separately, the change in curvature was measured after the Sn layer was removed by chemical etching. The difference in the curvature between the bilayer Cu/Sn structure and the same structure after etching off the Sn provides the average stress in the Sn film alone. Commercially available Rohm and Haas Tin Strip Solution 3006 (consisting of 400 g 70% nitric acid, 19 g sulfamic acid, 13 g fluoroboric acid, and 596 g DI water) was used to strip the Sn layer. The samples were dipped in the solution for 15 s, rinsed twice in DI water (30 s each), and dried with a flow of compressed nitrogen.

Transmission electron microscopy (TEM) was used to characterize the microstructure of the vapor-deposited material. Plan-view examination of the films involved depositing pure Sn (150-nm-thick films) as well as a Cu/Sn bilayer (100-nm Cu and 600-nm Sn) on special $SiO_2$ membrane TEM grids. These grids are 3 mm in diameter, 200 $\mu$m thick, and contain a 0.5-mm square slotted window in the center; this window contains a 50-nm-thick $SiO_2$ membrane across it. The bilayer specimens were immersed in the Sn stripping solution (described above) to dissolve the Sn layer so that the intermetallic formed at the Cu/Sn interface could be characterized without interference from the Sn layer. Energy-dispersive x-ray (EDX) analysis and electron diffraction were used to identify the phases present. Nevertheless, interference from the base Cu layer is still present. Thus, carbon extraction replicas were obtained to unambiguously characterize the intermetallic phase. This technique is commonly used to characterize carbides in steels[44] but, to the best of our knowledge, has not been utilized for studying Cu–Sn alloys previously. Here, to ensure a clean, oxide-free surface, the tin-stripped samples were briefly re-immersed into the commercial tin strip solution (for 10 s), rinsed in DI water, and dried with a flow compressed nitrogen. A carbon coating of 5 nm was then deposited onto the specimens with a Bal-Tec CED 030 carbon evaporator (with a single thread) in a vacuum of $1.33 \times 10^{-6}$ Pa. The carbon-coated surfaces were then cut with a razor blade into 1.5-mm squares. The replicas were etched free from the substrates with a solution of 10% phosphoric acid in DI water (5 V for approximately 5–10 s, using a copper anode) and then captured on 200-mesh copper grids for TEM examination.

Cross sections of the bilayered Cu–Sn specimens that had been deposited on an epoxy substrate were examined under TEM after different time intervals (1 h, 5 days, 31 days, and 48 days after deposition) to understand the nature of the stress relaxation processes that controlled the kinetic measurements. The cross-section samples were prepared using an ultramicrotome (Reichert-Jung Ultracut E microtome fitted with a Diatome diamond knife with a 45° cutting angle, operated at a slow cutting speed of 0.7 mm/s). Upon cutting, the 40- to 90-nm-thick samples were floated off into water and collected on 200-mesh gold TEM grids. This approach avoided the difficulties of preparing the soft Sn sample by polishing and prevented the ion damage and Ga contamination that can be induced by focused ion beam (FIB) preparation.[45] The films were grown on an epoxy substrate (rather than a Si wafer) to prevent damage to the microtome diamond knife. To determine the possible effects of the epoxy substrate on the Cu microstructure and hence on the interfacial reaction between Sn and Cu, a specimen was produced with the Sn deposited on the epoxy first and the Cu on top of the Sn (i.e., reversal of layer sequence). The interfacial reaction did not appear to be affected in any way, and this was taken to indicate that the epoxy substrate did not influence the reaction between the Cu and Sn in any substantial and/or recognizable manner.

## III. RESULTS

### A. Stress evolution

Stress evolution in Sn in the Cu/Sn bimetal film deposited on a Si substrate as a function of time is presented in Fig. 1 for a bimetal film consisting of 1200-nm Sn on 600-nm Cu. In the early stages, the composite film (diamond symbols) shows a net tensile response that reaches a maximum and then decreases with further time; the rate of decrease is initially rapid but then slows down for longer times. This measured curvature includes effects of stress in both the Sn and Cu layers. By measuring the difference in the curvature between the full Cu/Sn structure and the same structure after the Sn has been chemically etched off, the average stress in the Sn film alone

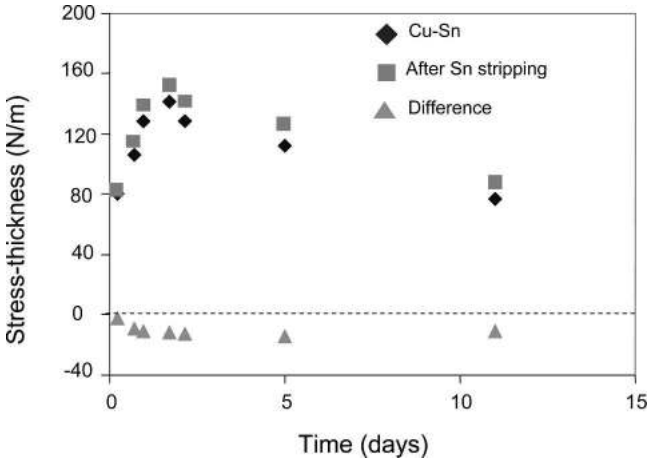


FIG. 1. Stress evolution with time measured using MOSS in the vapor-deposited samples (PVD) 1200-nm Sn/600-nm Cu bimetal films, after stripping the Sn in each instance, and the difference denoting the stress × thickness in the Sn layer and its evolution with time.

was obtained (triangle symbols). Measurement from multiple samples was used to obtain the stress evolution with time. It is seen that the stress in the Sn film is compressive, initially increasing with time and then reaching, more-or-less, a steady state at longer times.

### B. Microstructure characterization

TEM of the bilayer Sn–Cu samples is complicated by interference between features in the different layers. To characterize the as-deposited and evolving microstructures, we describe below the results of several different types of measurements. Plan-view measurements were made of pure Sn layers to determine the microstructure of the Sn grains. Plan-view measurements of Sn–Cu bilayers were made after etching to remove the unreacted Sn component. Carbon extraction replicas were also used to separate the intermetallic particles from the underlying matrix. Cross-sectional measurements were made at different times after deposition to capture the microstructure of the Sn layer and the growing intermetallic particles.

#### 1. Plan-view examination

Representative bright-field images of single layers of 150-nm-thick Sn film deposited on a $SiO_2$ membrane grid are shown in Figs. 2(a) and 2(b). The Sn grains are fairly large (~200–700 nm) and contain several subgrain boundaries, as demarcated by the arrays of dislocations. The interiors of the grains and subgrains are essentially dislocation-free. It is likely that dynamic recovery proceeds during and after the deposition process as room temperature is of the order of $0.6T_m$. Similar microstructural features were also observed when the Sn was deposited on a NaCl single-crystal substrate, floated off in water, lifted onto a Cu grid, and observed in the microscope.

The microstructure after the Sn was etched away from the Cu/Sn bilayer deposited on the $SiO_2$ membrane reveals the presence of an intermetallic phase as early as 3 h after deposition [Fig. 3(a)]. The mottled background in Fig. 3(a) is the underlying Cu layer, and a higher-magnification image shows the Cu to be composed of nanocrystalline grains [Fig. 3(b)] which are often twinned. The islands/discontinuous networks of a second phase exhibiting the dark contrast in Fig. 3(a) were found to contain Cu and Sn by EDX and are thought to be the $Cu_6Sn_5$ intermetallic phase that forms due to reaction between Cu and Sn at the Sn grain boundaries. Careful

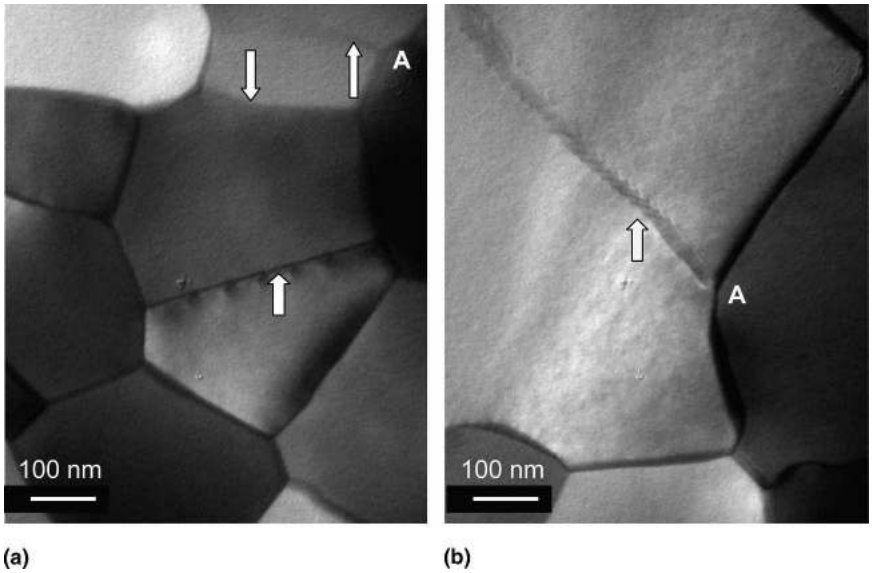


FIG. 2. (a, b) Representative micrographs (plan view) of 150-nm-thick Sn film deposited on $SiO_2$ membrane showing submicron, dislocation-free grain interior, and occasional subgrain boundaries (indicated by white arrows).

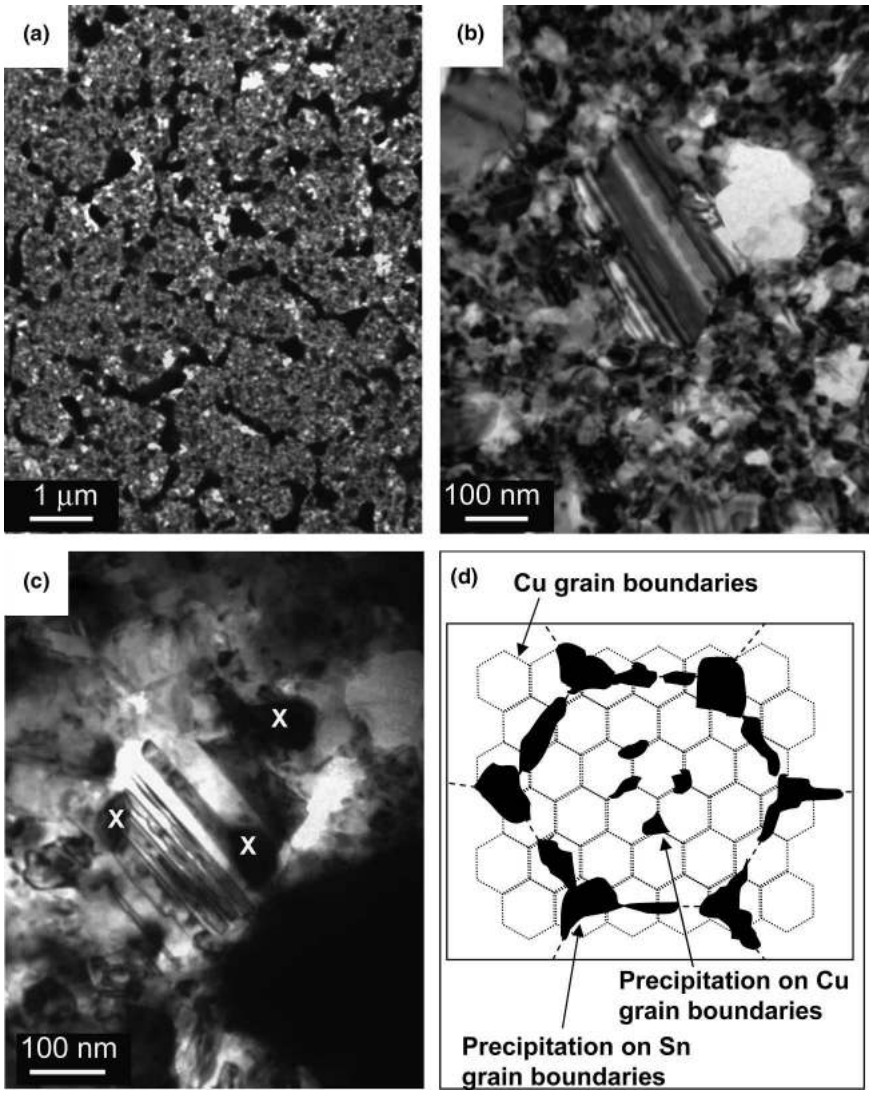


FIG. 3. Plan-view microstructure after etching away the Sn of the Cu/Sn bilayer deposit on the $SiO_2$ membrane revealing (a) the presence of the $Cu_6Sn_5$ intermetallic phase as early as 3 h after deposition, its morphology demarcating the original Sn grain boundaries, (b) the underlying nanocrystalline Cu grains, often twinned, (c) the precipitation of the intermetallic phase (marked "X") at the Cu grain boundaries, and (d) a schematic summarizing the microstructural observations in (a)–(c).

examination of Fig. 3(a) as well as observations of the Cu grains at higher magnification confirms the presence of $Cu_6Sn_5$ particles at the Cu grain boundaries [Fig. 3(c)]. In Fig. 3(c), the Cu grain is recognized by the twins spanning the grain, and its chemistry was confirmed using EDX. Decorating the Cu grain boundaries are fine, discrete particles [such as those marked as "X" in Fig. 3(c)] and EDX data of these particles compared to an adjacent particle-free location in the Cu grain confirms that the particles contain Sn and are likely Cu–Sn intermetallics (due to the interference from the underlying Cu substrate, quantitative EDX is unreliable and diffraction data are complicated by significant overlapping of Cu and $Cu_6Sn_5$ peaks). Based on these observations, we conclude that the Cu–Sn intermetallics precipitate rapidly at the Sn grain boundaries in contact with the Cu/Sn interface, but to a lesser extent also at the Cu grain boundaries that are in contact with the Cu/Sn interface. A schematic illustration of the microstructure evolution as a consequence of the reaction between Cu and Sn is included in Fig. 3(d).

To further investigate the structure and composition of the intermetallic particles, single-stage carbon extraction replicas were obtained from the Cu/Sn bilayer specimens (600-nm Cu/1200-nm Sn) deposited on Si wafer substrates after the Sn had been chemically etched off as previously described. These replicas contain the intermetallic particles but are now free of Sn and the underlying Cu layer and permit unambiguous identification of the intermetallics. A bright-field image from a replica confirms successful extraction of the intermetallic particles [Fig. 4(a)] and an associated electron diffraction ring pattern matches well with the simulated pattern [Fig.

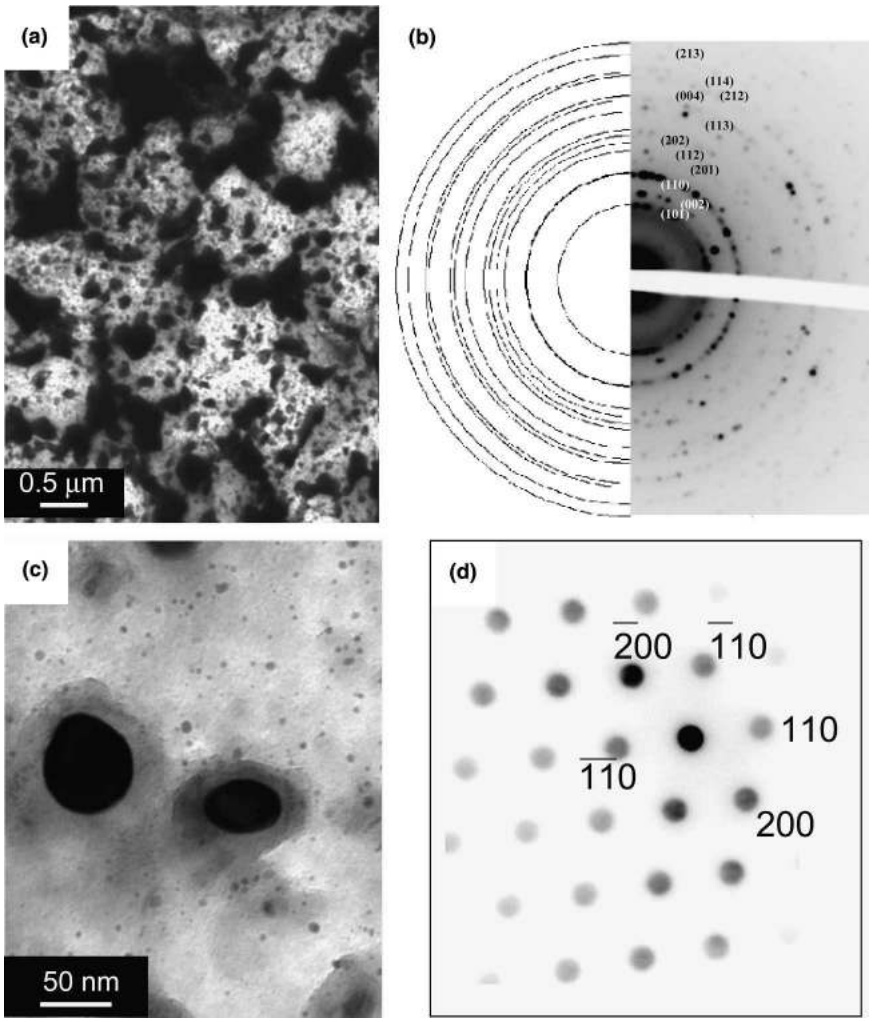


FIG. 4. (a) TEM image of a single-stage carbon extraction replica containing the $Cu_6Sn_5$ intermetallics (see Sec. II for procedural details), (b) the associated diffraction ring pattern confirming its structure and identity, (c) the fine, isolated intermetallic particles within the coarser network in (a), and (d) a microdiffraction pattern confirming it also to be $Cu_6Sn_5$.

4(b)] for $Cu_6Sn_5$. This pattern was obtained from an area that includes the coarse and fine intermetallic particles (i.e., those at the Sn grain boundaries as well as those at the Cu grain boundaries). Microdiffraction patterns [Fig. 4(d)] from the fine individual particles located in the interior of the network of intermetallics [Fig. 4(c)] were also consistent with $Cu_6Sn_5$.

Returning to the discussion of the membrane TEM specimens, it should be noted that the as-deposited Cu/Sn bilayer (100-nm Cu + 600-nm Sn) was too thick to be electron-transparent prior to the Sn being stripped off. Previous attempts to characterize the microstructure by viewing through thinner electron-transparent bilayers of Cu and Sn (e.g., 50-nm Cu and 100-nm Sn, vapor-deposited on a NaCl single crystal and subsequently floated off on water and retrieved on a Cu grid) proved to be futile; the microstructure was complicated by the overlapping of features through the foil thickness that precluded isolation and identification of crystallographic and microstructural details unambiguously. Thus, characterizing the Sn microstructure on Cu requires cross-section TEM analysis.

### 2. Cross-section examination

As described in Sec. II, cross-sectional Sn/Cu bilayer specimens suitable for TEM examination were obtained using an ultra-microtome, and representative images of the cross-section from a specimen soon after deposition (1 h) are shown in Figs. 5(a)–5(d). A low-magnification TEM image [Fig. 5(a)] illustrates that the Sn grains are columnar and vary in width from 0.3 to 1 μm, whereas the Cu grain diameter is on average in the range of 50–100 nm. Higher-magnification images of the Cu/Sn interfacial region [Figs. 5(b) and 5(c)] confirm the presence of a few intermetallic particles, indicated by arrows and their identity was confirmed using electron diffraction and chemical analysis (SAD and EDX). For the most part, these intermetallic particles were located at the

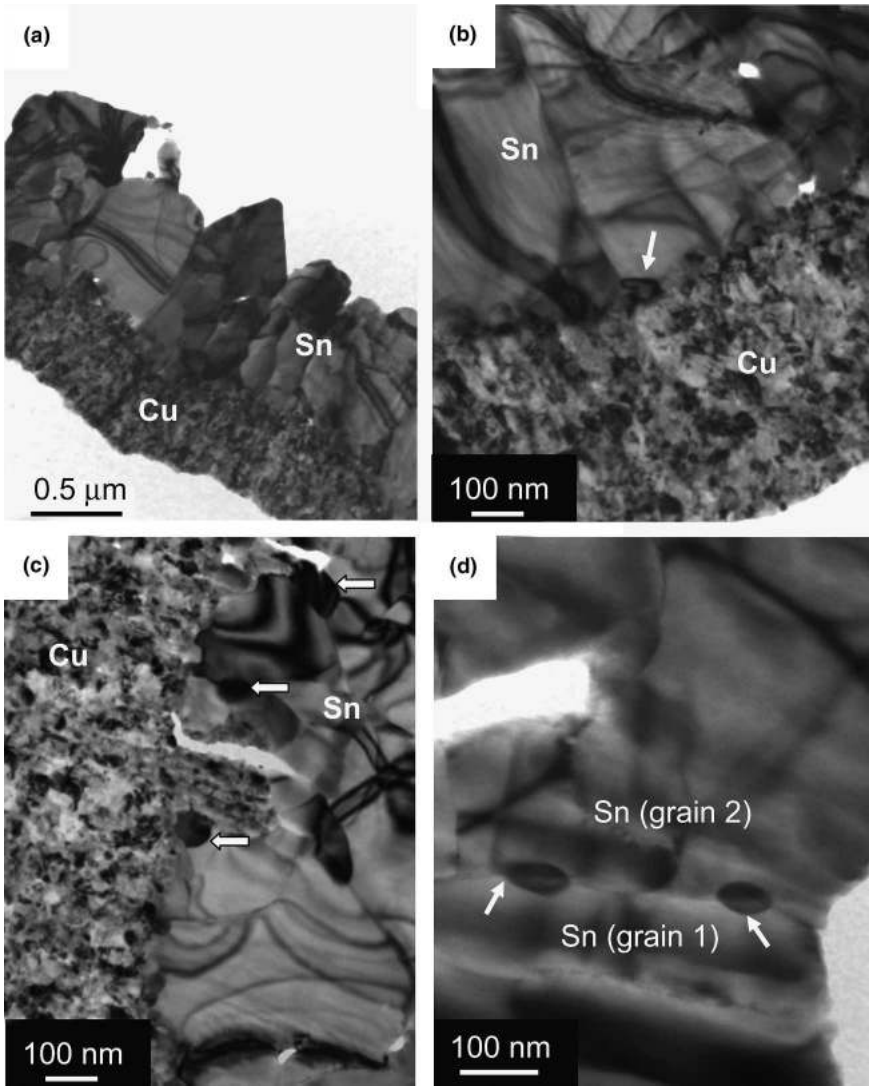


FIG. 5. Cross-sectional view of the Cu/Sn bimetal film deposited on an epoxy substrate about 1 h after deposition. (a) Ultra-fine Cu grains and the columnar coarser Sn grains are seen, and (b, c) higher-magnification images of the interface confirm the occasional presence of the intermetallic phase (white arrows) at locations where the columnar Sn grain boundaries meet the Cu/Sn interface. (d) Presence of discrete particles of the $Cu_6Sn_5$ phase further up along the Sn grain boundaries is illustrated (although this was rare).

junction where the columnar Sn grain boundaries met the Cu/Sn interface; occasionally, however, isolated intermetallic particles were also observed at the Sn grain boundaries away from the Cu/Sn interface [Fig. 5(d)], suggesting rapid diffusion of Cu along the Sn grain boundaries.

In addition, examination near the top surface of the Sn grains at high magnification confirms the presence of a distinct, adherent 5- to 8-nm layer that appears amorphous and is thought to be Sn oxide [Figs. 6(a) and 6(b)]. The fine scale precluded reliable direct evaluation of the composition of the layer, but the dimensions are in reasonable agreement with a recent report from Sobiech et al.,[46] where a tin oxide thickness of 2–3 nm was claimed on the basis of XPS sputter-depth profiles.

Five days after deposition, a second slice was obtained from the same bilayer sample and examined in the microscope [Figs. 7(a) and 7(b)]. The intermetallic layer in this specimen was almost continuous at the Cu/Sn interface [Fig. 7(a)], and in addition, where larger particles were present, it was evident that dislocations were being punched into the Sn grains [Fig. 7(b), illustrated by white arrows] from the $Cu_6Sn_5$/Sn interface, presumably to relax the misfit stress arising from the growth of these particles. Another interesting observation is the presence of a subgrain ahead of the particle, and the subgrain boundaries are seen to emanate from the particle/Sn matrix interface. This is strongly suggestive of rapid rearrangement of these misfit dislocations to form these subgrain boundaries, and indicative of dynamic recovery, a phenomenon that is usually evidenced in metals being plastically deformed at temperatures around $(0.5–0.7)T_m$. As previously mentioned [Figs. 6(a) and 6(b)], at the Sn

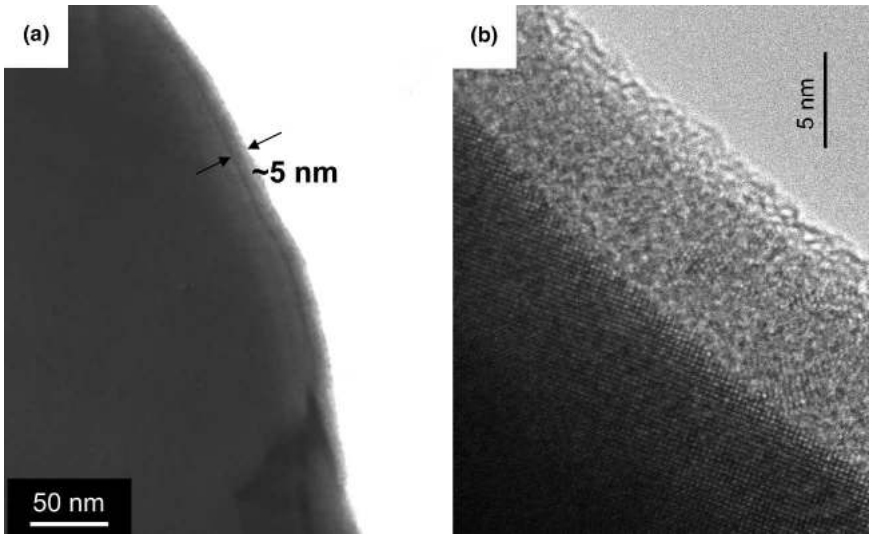


FIG. 6. (a) Cross-sectional view of the upper portion of the columnar Sn grain confirms the presence of an approximately 5-nm-thick region thought to be the tin oxide layer; (b) high-resolution image confirming the crystalline Sn below it; the top layer itself appears amorphous. The interface appears adherent and continuous.

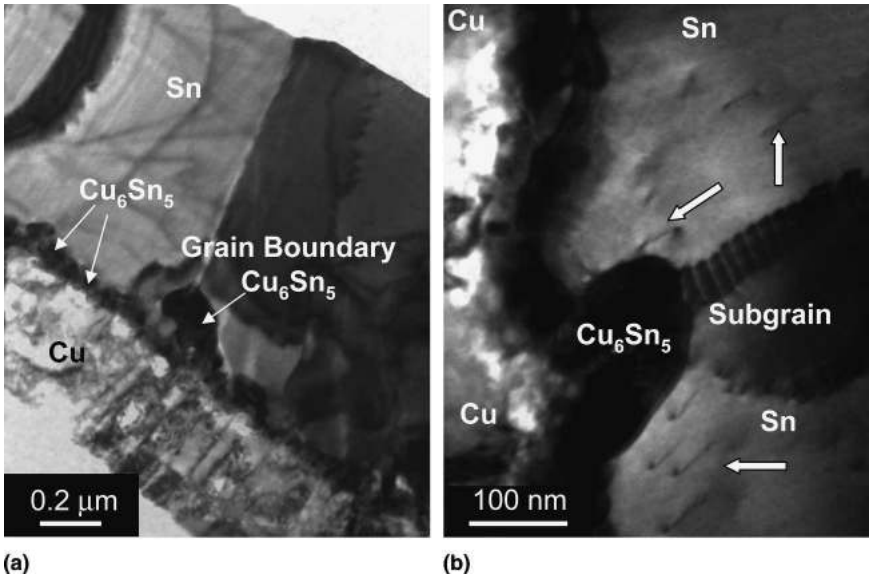


FIG. 7. Cross-section of the Cu/Sn bilayer deposited on the epoxy, 5 days after deposition. (a) Continuous rough layer of $Cu_6Sn_5$ is observed along the Cu/Sn interface, the coarse size being present at locations where the Sn grain boundaries meet the Cu/Sn interface; (b) higher-magnification image confirms dislocations being emitted from the $Cu_6Sn_5$/Sn interface into the Sn grain (white arrows) and the presence of a subgrain boundary at the interface.

surface, more than 1000 nm away from the Cu/Sn interface and the intermetallic particles, a fairly uniform 5- to 8-nm adherent surface oxide layer is seen in most locations. Where the oxide layer is present, dislocations appeared to stagnate in the Sn grain in the vicinity of the oxide layer, their configuration suggesting pileup and repulsion by the hard oxide layer; two examples are shown in Figs. 8(a) and 8(b). In contrast, when the oxide layer is absent (possibly due to handling; the reformed oxide may be thin enough that the stress field due to the dislocation is adequate to break it off in the microscope), dislocations are readily drawn to the free Sn surface and eliminated. This is evident in the two time-sequential images shown in Figs. 8(c) and 8(d), the process being encouraged by focusing and defocusing the incident beam. This confirms that one mechanism by which stress may be felt at the Sn surface is by dislocation pileup at the oxide layer at the Sn surface.

One-month after deposition, an additional slice was obtained to examine the microstructural evolution at longer times; the results are illustrated in Figs. 9(a)–9(d). The low-magnification image of the bilayer cross section

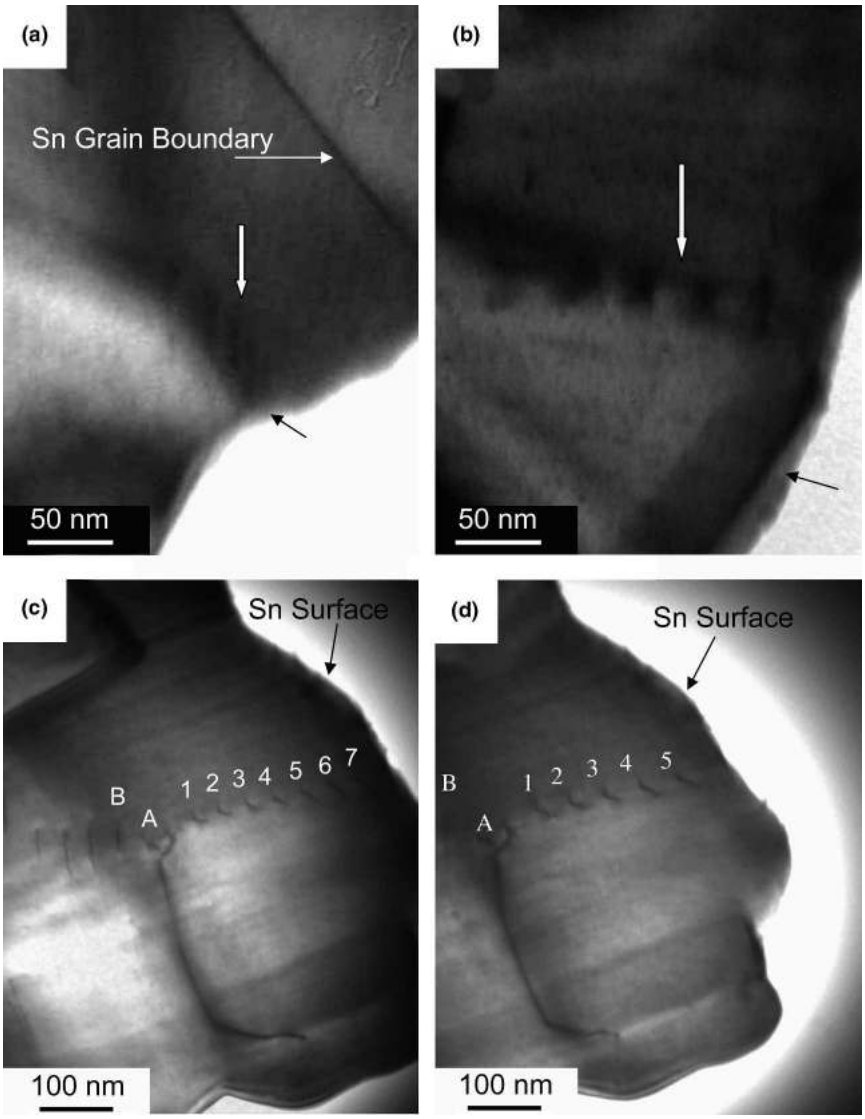


FIG. 8. (a, b) Two instances of dislocation pileup at the Sn surface where Sn oxide was observed; (c, d) images reflecting two snapshots in time, in which an array of seven dislocations is seen in (c); (d) by focusing and defocusing the beam, they could be made to glide out the surface, leaving behind only five of the original seven dislocations.

[Fig. 9(a)] confirms the growth of the intermetallic phase as fine columns, the extent of growth being higher at the Sn grain boundary relative to the Sn grain interior. A higher-magnification image of the intermetallic confirms each of the columns to be polycrystalline, with the grain size being on the order of 30 nm; the polycrystalline nature is also confirmed by the diffraction ring pattern obtained from this region [inset, Fig. 9(b)], and its identity is verified as $Cu_6Sn_5$. To the best of our knowledge, such high-resolution imaging of the morphology of the intermetallic phase has not yet been reported. A careful examination of the $Cu_6Sn_5$/Sn interface in Fig. 9(c) confirms the cusping of the individual columns at triple junctions as mandated by surface tension balance. Rather interesting are the two locations at the interface marked "A" and "B," where the interface appears to be "further drawn" into the Sn; at these locations, tilting experiments confirm the presence of individual arrays of dislocations constituting a subgrain grain boundary in the Sn. We suspect that dislocations punched out ahead of the interface have had an opportunity to quickly rearrange to form the subgrain boundary (dynamic recovery), and the resulting surface tension balance has caused the interface to be drawn out, similarly to the phenomenon of serrated grain boundaries formed during creep in metals and alloys.[47,48] A schematic illustration is provided in Fig. 9(d) to visually capture the description of the intermetallic morphology and the advancing interface configuration described above. EDX spectra from the Cu, Sn, and the $Cu_6Sn_5$ regions are shown in

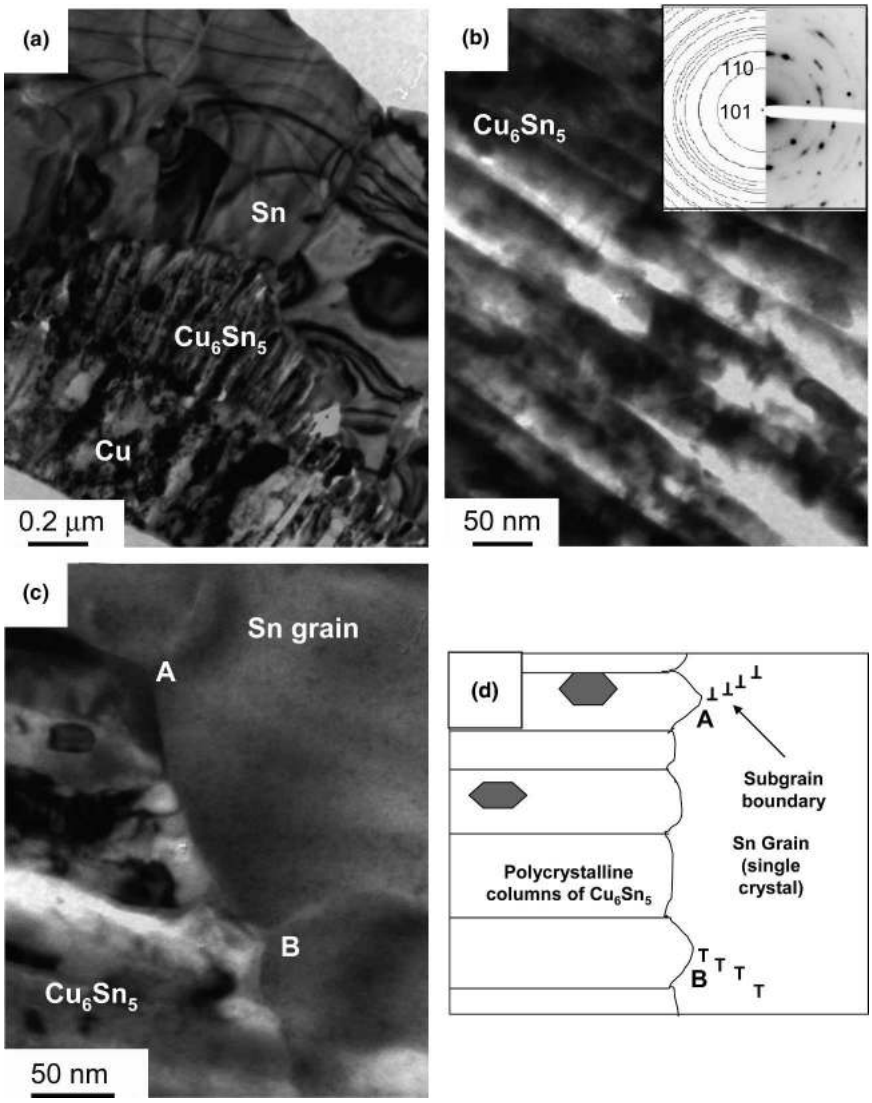


FIG. 9. Cross section of the Cu/Sn (Sn on top) bimetal film 1 month after deposition. (a) Low-magnification image showing the columnar morphology of the $Cu_6Sn_5$ intermetallic evolving from the interface, the extent of growth being higher at the Sn grain boundary than the grain interior; (b) higher-magnification image confirming the columnar structure and the polycrystalline nature of the individual columns; (c) microcusping of the $Cu_6Sn_5$/Sn interface at the column triple junctions and additional interface shape modification due to the interaction of the interface with subgrain boundaries in the Sn at locations A and B; (d) schematic summarizing the microstructural features observed in (a)–(c).

Figs. 10(a)–10(c), confirming the compositions of these three regions.

Forty-five days after deposition, another cross-section slice was obtained and images are shown in Figs. 11(a)–11(d). In Fig. 11(a), the ends of two adjacent columns of $Cu_6Sn_5$ are visible in the upper left corner, and the conical tip of each column can be seen associated with a subgrain boundary in the Sn grain ahead of the $Cu_6Sn_5$/Sn interface. Further into the Sn grain, several subgrain boundaries can be readily seen. Such subgrain boundaries are found even near the Sn-free surface [Fig. 11(b), labeled "1" through "5"], and in some instances, the subgrain boundaries intersect the Sn free surface [Fig. 11(c)]. Where they intersect the free surface, to maintain surface energy balance at the node, the free surface is "pulled inward" by the subgrain boundary and this is evident in Fig. 11(c). The misorientation resulting between the subgrains as well as the "cusping" that results from subgrain intersection with the Sn surface can provide opportunities for cracking of the thin Sn oxide at the surface. Furthermore, subgrain boundaries also serve as dislocation sources; an example of this is shown in Fig. 11(d). This can also lead to extensive pileup of dislocations at the Sn surface when an oxide layer is present and causes local stresses at the head of the pileup. Thus, the plastic deformation of the Sn grain provides multiple opportunities to generate stress at the Sn surface that can then break the Sn oxide layer.

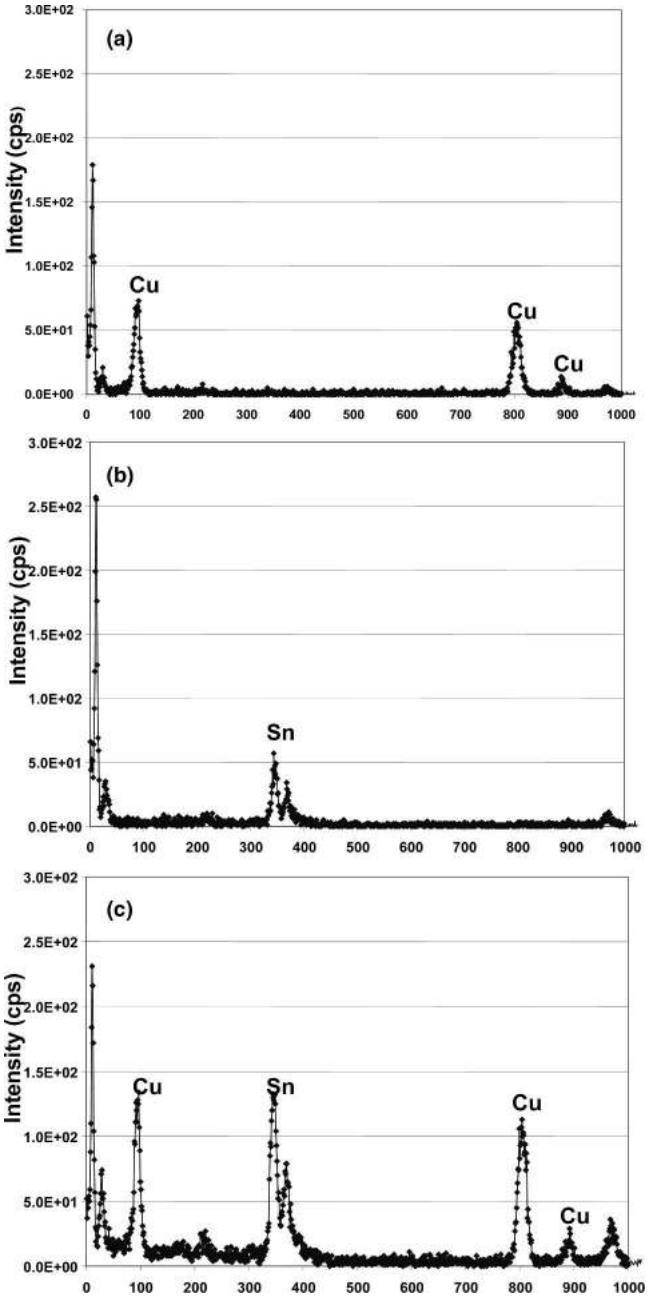


FIG. 10. EDX spectra taken from the (a) pure Cu, (b) pure Sn, and (c) columnar regions in Fig. 9(a), confirming the compositions of the individual regions.

To verify that the epoxy substrate on which the Cu layer was deposited does not influence the interfacial reaction, a specimen was prepared with the layer sequence being reversed (i.e., Sn on the epoxy layer and Cu above the Sn), and a cross section of the specimen was examined in the TEM 5 days after deposition. Representative micrographs [Figs. 12(a) and 12(b)] confirm that the layers continue to react and form $Cu_6Sn_5$ along the interface in the same manner as the Sn-top, Cu/Sn bilayer specimen.

Lastly, whisker formation is verified in the SEM images shown in Figs. 13(a) and 13(b). These images were obtained from the same samples that were used to obtain the cross-section TEM slices and confirm that depositing on the epoxy substrate does not affect the evolution of whiskers. In Fig. 13(a), the whiskers are shown evolving on the Sn surface, but perhaps more intriguing is the fact that Sn whiskers even extrude out through the Cu-top specimen [Fig. 13(b)]. We have also seen this phenomenon occur in PVD bimetal layers on hard substrates such as silicon. EDX analysis confirms these whiskers emanating on the Cu surface to be pure Sn whiskers, sometimes with a plug of Cu on top where they pushed through the copper layer.

## IV. DISCUSSION

### A. Consideration of sample preparation effects

Prior to engaging in a discussion of the significance of the electron microscopy observations, it is necessary to consider the validity of the observations. This is necessitated by the facts that Sn is a soft, low-melting material that is in contact with a harder intermetallic phase ($Cu_6Sn_5$) at the Cu/Sn interface and the TEM cross-section specimen preparation involves mechanical cutting (albeit microtoming); furthermore, beam heating contributing to both thermal-expansion mismatch between the Sn and the $Cu_6Sn_5$ as well as to dislocation motion and rearrangement needs consideration. Examination of Figs. 2(a) and 2(b) confirms the presence of subgrain boundaries and the absence of matrix dislocations in the columnar Sn grains deposited on the $SiO_2$ membrane TEM grid. This specimen did not experience any cutting or mechanical force, and the source of dislocations is thought to be deposition stresses; rearrangement of dislocations to form subgrain boundaries is thought to occur prior to specimen insertion in the microscope. The latter conclusion is due to the fact that at locations where the dislocation array meets the grain boundary ["A" in Figs. 2(a) and 2(b)], a triple junction node is present with the Sn grain boundary conforming to surface tension balance requirements. Such events of grain boundary node migration and reconfiguration were never observed to occur in the microscope. Thus it appears that dislocations can be generated and rearrange without mechanical stress being applied by cutting, etc.

The cross-section TEM specimens (Figs. 5, 7, 9, and 11) were obtained following various lengths of time after deposition (1 h, 5 days, 30 days, and 45 days), and the population of subgrain boundaries present in the Sn grain increased dramatically in them, suggesting that they were formed and reconfigured prior to cutting. More importantly, in Figs. 9(c) and 11(a), the serrated appearance of the interface between the $Cu_6Sn_5$ columns and the adjacent Sn—with the tip of the serration being associated

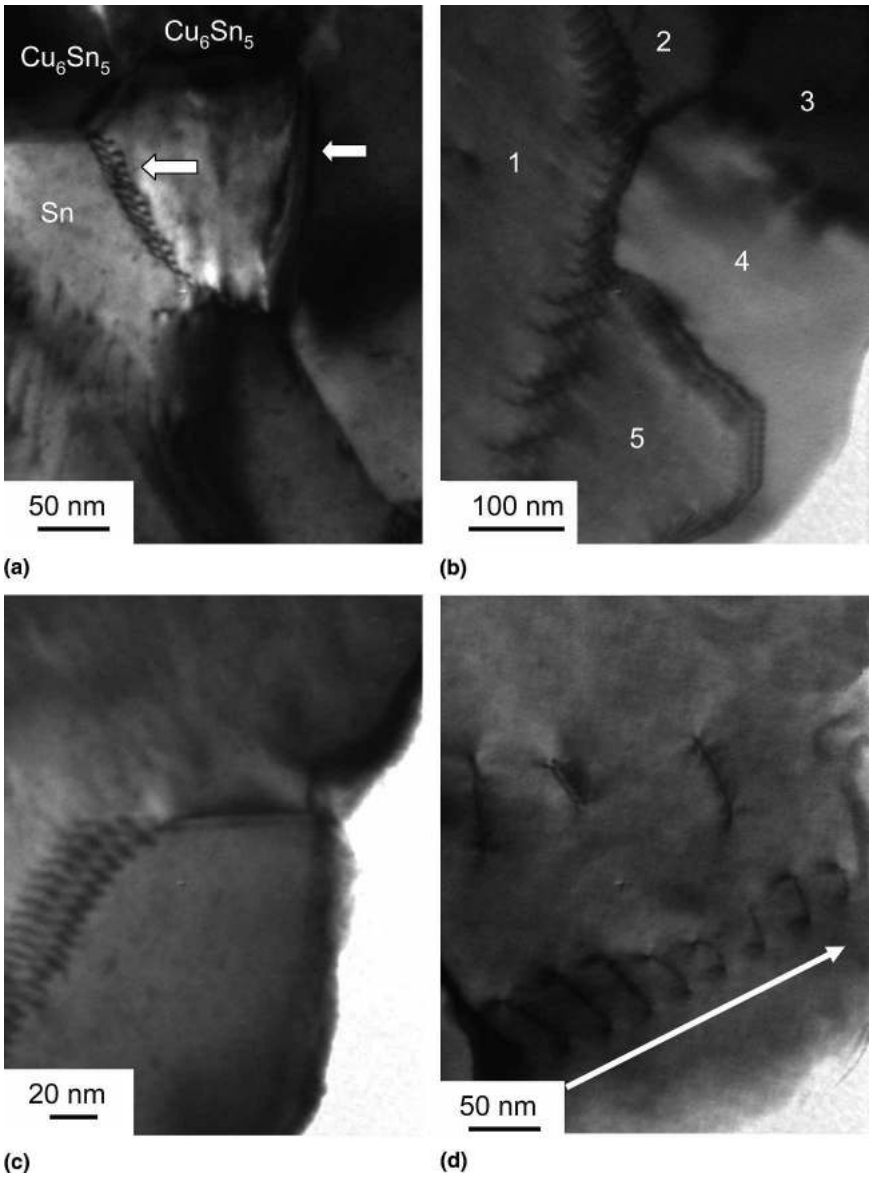


FIG. 11. High-magnification images of the cross section of Sn grains ahead of the advancing $Cu_6Sn_5$/Sn interface, 45 days after deposition showing the (a) microserrated interface configuration associated with the subgrain boundaries ahead of the interface; (b) presence of a significant number of subgrains in the Sn (labeled 1–5) extending to the Sn surface; (c) intersection of a subgrain boundary with the Sn surface producing local surface cusping; and (d) glide dislocations emanating from a subgrain boundary dislocation source near the surface, that can then pile up at the surface.

with a subgrain boundary—is indicative of this configuration occurring prior to cutting rather than due to the cutting or due to beam heating in the microscope. For these reasons, we believe that the observed microstructural evolution is not a consequence of specimen preparation.

### B. Relation of dislocation motion to stress generation at the Sn surface

These studies therefore directly confirm the presence of plastic deformation (dislocation activity) in Sn grains arising from the formation of the intermetallic phase and the resulting misfit strain. The continuous generation of misfit dislocations, their motion through the Sn grains, and their piling-up at the Sn surface due to the presence of an oxide layer provide a plausible explanation for how strain in the region around the growing intermetallic particles can be felt at the Sn surface. This overcomes the deficiency of models based on purely elastic-strain effects, since elastic-strain fields are short-range and cannot account for these long-range effects. Stress at the Sn surface has also been attributed to diffusional creep,[14] which may occur, but electron microscopy cannot directly confirm the contribution from this mechanism. In this context, it is pertinent to recognize that the dislocations

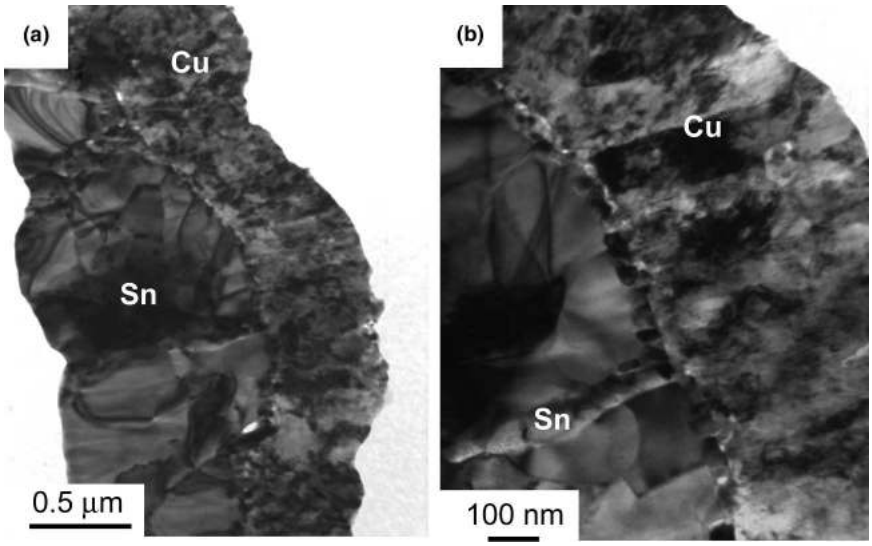


FIG. 12. (a, b) Cross-section of the Cu/Sn bimetal layer deposited on epoxy with the Cu on top confirming the formation of intermetallic particles at the Cu/Sn interface that appears no different from the situation where the Sn was the top layer. The images were taken 5 days after deposition, and the intermetallics appear to be growing into the Sn layer.

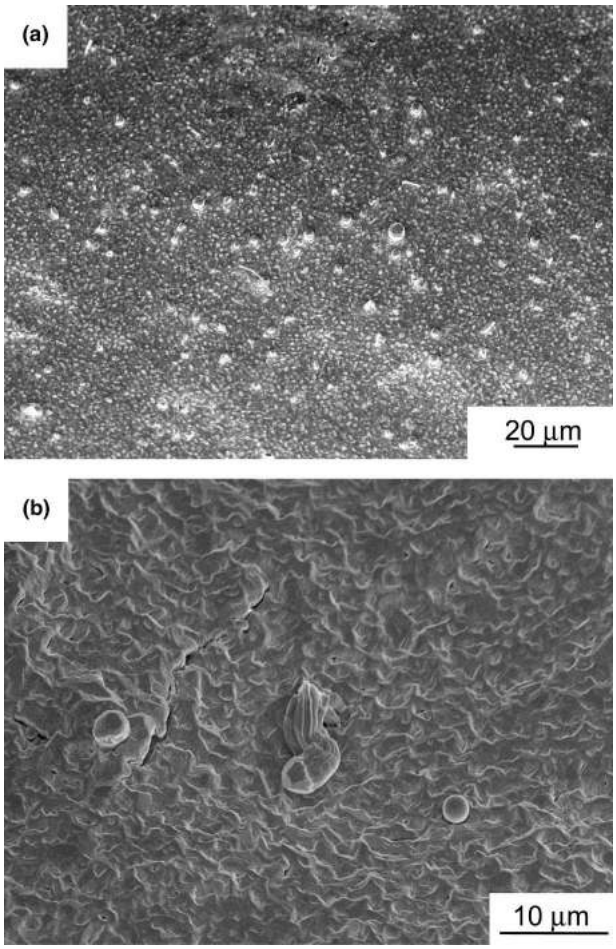


FIG. 13. Whisker evolution from (a) the Sn surface of the Cu/Sn bilayer deposited on epoxy from which all the cross-section samples were obtained; (b) curiously, Sn whisker evolution from the Cu surface of the Cu-top Cu/Sn bilayer specimen deposited on epoxy.

generated due to misfit strains at the intermetallic/Sn interface in the early stages after deposition may not necessarily glide all the way to the Sn surface as there may not be adequate stresses to sustain glide over such large distances. However, formation of the $Cu_6Sn_5$ intermetallic at the Sn grain boundaries can generate excess Sn atoms that can diffuse up the columnar grain boundaries toward the Sn surface. This process can generate a compressive biaxial stress on the Sn grains of sufficient magnitude and enable motion of the already generated dislocations or generate additional dislocations that can reach the Sn surface.

One important consequence of the dislocation activity is generation of stress at the Sn surface which is necessary to crack the Sn oxide, often considered a first step toward whisker evolution. However, the dislocations that are continuously ejected from the interface to accommodate the misfit strain also encounter vacancies and can climb (room temperature is $0.6T_m$ for Sn), and this enables rapid rearrangement of these dislocations into lower-energy arrays constituting subgrain boundaries. It was shown in Fig. 11(d) that these subgrain boundary dislocations can also serve as a dislocation source and produce slip dislocations that can rapidly pile up at the surface when the subgrain boundary source is in the vicinity of the surface. In some instances, subgrain boundaries can intersect the thin tin/tin oxide surface and produce a cusp at the surface [Fig. 11(c)], which then places a local stress on the stiffer oxide and can conceivably produce oxide cracking by delamination at the interface. Another important geometric aspect to consider is the formation of subgrains within the initially single-crystal columnar Sn. As subgrains form, separated by arrays of dislocations, misorientation develops between adjacent

regions, varying from as little as 0.25° to as high as 2–3°, depending on the type and spacing of dislocations forming such boundaries. Such local rotations could conceivably produce surface roughening and therefore serve as a means to crack the surface oxide. An example of three subgrain—and the misorientation between them obtained by diffraction methods—is shown in Fig. 14. A schematic illustration of the microstructural evolution discussed above is depicted in Fig. 15(a), emphasizing how these processes may produce stress at the Sn surface.

The motion of dislocations is also consistent with the stress-evolution kinetics observed in the curvature measurements. Even at the very early stages, a plastic zone is created in the vicinity of the intermetallic/Sn interface to relieve the misfit stress around the growing intermetallic particles. In the plastic zone, the stress has reached the flow stress of Sn, while further away from the interface, elastic deformation is present and decays rapidly.[41] The change in curvature due to Sn removal is indicated by the triangles in Fig. 1 and provides a measure of the stress evolution in the Sn layer. The increase in compressive stress (stress × thickness) observed in Fig. 1 is interpreted as the transient region where the elastic–plastic zone is in the process of spreading over the entire Sn layer thickness; the "steady-state" plateau stress is interpreted as corresponding to the plastic zone (with negligible work hardening) engulfing the entire Sn layer. As seen in Fig. 1, after about 1–2 days, the compressive stress in Sn reaches more-or-less a steady state of approximately 8 MPa, which is in line with that reported for the yield stress of Sn at room temperature.[49,50]

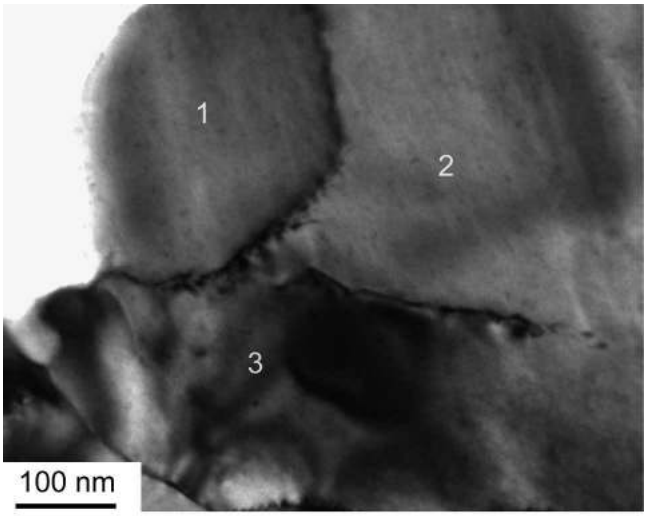


| | Misorientation (degrees) |
|---|---|
| Subgrains 1 and 2 | 1 |
| Subgrains 2 and 3 | 2 |
| Subgrains 1 and 3 | 1 |

FIG. 14. Misorientation measurements between three subgrains (labeled 1, 2, and 3) within a Sn grain in a Cu/Sn bilayer film.

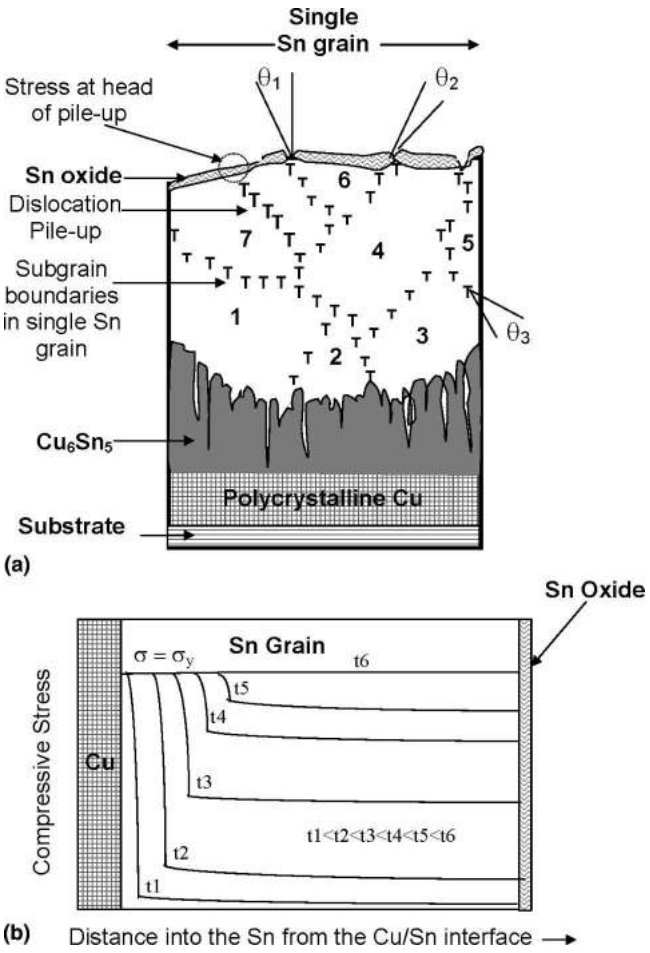


FIG. 15. (a) Schematic illustration of the various dislocation-related mechanisms observed in this study and how they might generate stress at the surface Sn oxide layer and crack the oxide. This step then becomes a precursor for whisker evolution. (b) Schematic profile at the continuum level illustrating how stress evolves with time in the Sn grain due to intermetallic growth (here, $\sigma_y$ is the yield stress of Sn) and as a consequence of excess Sn diffusion along the grain boundaries to the Sn surface.

A schematic illustration of stress evolution across the Sn grain is shown in Fig. 15(b), where the plastic layer (i.e., reaching a value of $\sigma_y$, the yield stress) spreads throughout the Sn layer thickness as time progresses and the intermetallic grows. In Fig. 15(b), we emphasize the nature of plastic deformation evolution. Although the region immediately ahead of the intermetallic/Sn interface has reached the yield stress due to misfit strain, and plastic deformation occurs and dislocations are emitted, except for the mutual repulsion of these dislocations, the stress to sustain their glide decays quickly as one moves away from the intermetallic/Sn interface and toward the

Sn surface. As a consequence, the plastic zone will advance, to a first approximation, only as fast as the intermetallic front advances into the Sn. However, migration of excess Sn up along the Sn grain boundary toward the Sn surface due to intermetallic formation at the Sn grain boundaries will produce longer-range biaxial compressive stresses in the Sn that can sustain the motion of the glide dislocations, activate new sources in the subgrains (or elsewhere), and fairly rapidly lead to the entire grain deforming plastically.

Although our experiments do not provide direct observations of diffusion, the deformation behaviors of single-crystal and polycrystalline Sn and of polycrystalline Sn alloys (e.g., Sn–Ag, and Sn–Pb–Ag) have been studied as a function of temperature and strain rate in the vicinity of room temperature, and the underlying mechanisms have been documented.[51–54] Thus, McCabe and Fine[51] have examined the creep response of 99.86% pure Sn and confirm pipe-diffusion–controlled climb at room temperature with a stress exponent of 8 and an activation energy of ~70 kJ/mol. Lattice-diffusion–controlled climb was reported for tests conducted in excess of 150 °C. Adeva et al.[52] conducted tensile tests on 99.9% purity Sn and concluded that the dominant plastic deformation mode was dislocation motion and that creep deformation was controlled by pipe diffusion, in agreement with the work of McCabe and Fine,[51] although the activation energy they measured was significantly lower than that reported in Ref. 51. A similar conclusion (i.e., pipe-diffusion–dominated climb in the temperature range from −50 °C to 150 °C) was reached by Lang et al.[53] based on their study of Sn–3.5%Ag alloy. Pao et al.[54] obtained steady-state creep properties from stress relaxation data; they reported an $n$ value for a 97Sn–2Cu–0.8Sb–0.2Ag alloy at 40 °C of 8.9 and concluded that the dominant underlying mechanism was dislocation glide/climb. From these studies, it is clear that plastic deformation by dislocation glide and dynamic recovery by climb are mechanisms to contend with when examining stress evolution and dissipation in Sn at room temperature, and the electron microscopy observations reported in this paper are certainly consistent with the observations in literature.

### C. Implications of intermetallic particle morphology on stress evolution

Obtaining quantitative estimates of the stresses induced by intermetallic formation is difficult because the stresses are strongly dependent on the morphology of the growing intermetallic layer and the deformation is strongly influenced by the details of the reaction kinetics. During the early stages, the intermetallic forms as isolated particles at triple junctions between Sn grain boundaries and the underlying nanocrystalline Cu layer, interspersed with smaller intermetallic particles at the intersection of Cu grain boundaries with the Sn overlayer. During the later stages, the intermetallic consists of a continuous but highly nonplanar layer. This produces two predominant wavelengths of roughness in the layer: a long wavelength comparable to the Sn grain size, together with a short wavelength roughness comparable to the grain size of the intermetallic.

The intermetallic forms as a result of copper diffusing from the substrate into the Sn layer (marker experiments show that the diffusion of Sn into Cu is negligible[13,14]). This depletes matter from the Cu, inducing a tensile stress that has been observed in our experiment. The Cu that migrates into the overlying Sn layer combines with Sn to form the intermetallic particles. This may occur as a result of adding Cu atoms to the existing Sn lattice, making the intermetallic particle much larger than the Sn it replaces. The increase in volume can be quantified by a volumetric transformation strain (analogous to a thermal expansion) with magnitude $\epsilon_0 = 0.13$. This expansion must be accommodated by elastic or plastic deformation in the surrounding Sn or in the particle. Alternatively, some fraction of the Sn atoms in the original lattice may be ejected into the surrounding material, allowing them to be replaced by Cu. In this case, a smaller transformation strain occurs in the intermetallic, but the atoms ejected into the surrounding Sn must be accommodated within the pre-existing lattice. The effect of this process is also similar to a thermal expansion and generates a compressive stress in the surrounding Sn. Gradients in this compressive stress would drive the ejected Sn to diffuse through the Sn film and eventually cause it to be accommodated at grain boundaries or at whiskers.

The fraction of atoms in the original Sn lattice that are replaced by Cu depends on the relative rates of diffusion of Cu and Sn; if Cu diffusion through the Sn were much faster than Sn self-diffusion or the interface reaction, then the volumetric strain in the intermetallic would approach the upper bound of $\epsilon_0 = 0.13$. If Sn diffusion were much faster than Cu diffusion or the interface reaction, the intermetallic particle would have the same volume as the Sn it replaced. The rates of diffusion are partly determined by the stress distribution resulting from the formation of the intermetallic; large (compressive) stresses would accelerate the diffusion of Sn away from the particle, and tend to reduce the transformation strain. If the stresses could be relaxed, e.g., by dislocation motion in the Sn, then Sn diffusion would be slowed and the volume change would increase within the intermetallic particle.

To appreciate the consequences of the morphology of the intermetallic, note that stress is generated in the Sn grains as a direct result of the nonplanar nature of the intermetallic. To see this, note that if (i) the intermetallic were to form as a perfectly planar layer and (ii) Sn diffusion is slow, then the Sn would remain stress free

(neglecting the small stress induced by substrate curvature), while a biaxial state of compressive stress would be generated in the intermetallic layer. If the (planar) intermetallic were to remain elastic, it would experience a stress given by $\sigma_{IMC} = -\epsilon_0 M_{IMC}$, where $\epsilon_0$ is the dilatational strain associated with intermetallic formation, and $M_{IMC} \approx 123$ GPa is the biaxial modulus of the intermetallic (the value for the biaxial modulus is taken from Ref. 21, $M_{IMC} = E/(1-\nu)$, where $E$ is the Young's modulus and $\nu$ is the Poisson's ratio; we use the biaxial modulus because the film is in a state of biaxial stress). For the limiting case $\epsilon_0 = 0.13$, this gives $\sigma_{IMC} = -16$ GPa. In practice, the stresses are far smaller than this estimate because the nonplanar morphology of the intermetallic and plastic flow in the surrounding Sn allows the stress to be relaxed.

In contrast, if the intermetallic develops as isolated particles, or a layer with nonuniform thickness, substantial stresses can be generated in the Sn. The detailed nature of the stress distribution can only be determined with the aid of numerical simulations, but some qualitative estimates can be made on the basis of solutions to simple elastic and elastic–plastic boundary value problems.

As a specific example, suppose that the intermetallic consists of an array of spherical particles, with radius $a$, and spacing $L$, that form within the Sn layer. If the Sn were to remain elastic, we would expect the stress in the Sn near the particles to be an approximately spherically symmetric stress state with origin at the center of the sphere. The expected magnitude of the radial and hoop components of stress at a distance $r$ from the particle can be estimated from the Eshelby solution as

$$\sigma_{rr} = -\sigma_0 a^3/r^3 \text{ and } \sigma_{\theta\theta} = \sigma_{\phi\phi} = \sigma_0 a^3/2r^3,$$

where $\sigma_0 = 2E\epsilon_0/3(1-\nu)$, and $E$ and $\nu$ denote the Young's modulus of the Sn and intermetallic (taken to be identical for this simple estimate). Taking $E \approx 50$ GPa, $\nu \approx 0.36$ for Sn, and with $\epsilon_0 \approx 0.13$ gives $\sigma_{rr} \approx 7$ GPa and $\sigma_{\theta\theta} \approx 3.5$ GPa at the particle/matrix interface. The stresses decay rapidly with distance from the particle, however. For a particle with a 50-nm radius, these stresses have values on the order of 1 MPa at the surface of a film that is 1 μm thick. Estimates of the stress state based on such simple elastic calculations are highly misleading because the predicted stresses greatly exceed the yield stress of Sn. As a result, they overestimate the magnitude of the stress near the intermetallic particles while underestimating the stresses far from the particles.

The stresses near the particle/matrix interface are more than sufficient to induce plastic flow in the tin. The radius of the plastic zone around the intermetallic particles can be estimated from the solution to an expanding spherical inclusion in an elastic–plastic matrix, which suggests that $c \approx a[\epsilon_0 E/Y(1-\nu)]^{1/3}$. Taking $Y \approx 8$ MPa for the yield stress of tin gives $c \approx 11a$. This suggests that a plastic zone will develop around the particles as they nucleate and will progressively spread through the tin grains as the particles increase in size. An array of particles with 100-nm radius and 1-μm spacing would be sufficient to cause yield throughout a tin film 1 μm thick. In practice, the plastic zone would likely be somewhat smaller than this simple estimate suggests, partly due to the constraining effect of the substrate and partly because plastic flow in small volumes is inhibited by a lack of dislocation sources and strain gradient hardening. Nevertheless, there is ample driving force for the dislocation nucleation and migration observed in experiment. In addition, the prediction is qualitatively consistent with the experimental observation that the stress in the Sn progressively increases as the particles grow and reaches a steady state value comparable to the compressive yield stress of Sn.

The plastic flow in the tin has a significant influence on the stress state: a crude estimate follows from the fields surrounding an expanding inclusion in an elastic–plastic matrix as $\sigma_{rr} = 2Y\log(r/c) - 2Y/3$ and $\sigma_{\theta\theta} = \sigma_{\phi\phi} = 2Y\log(r/c) + Y/3$. This estimate should be treated with caution, as interactions between particles and the constraining effect of the substrate would be expected to significantly modify the stress, but it illustrates the general trend that (i) stresses in the tin and intermetallic particles are likely to be of the order of the yield stress of Sn, in agreement with experimental observations; and (ii) stresses in the Sn decay more slowly than the elastic solution predicts. In addition, individual dislocations and dislocation pile-ups can induce large stress concentrations that could fracture the passivating oxide, as discussed in Sec. IV. B.

It is more difficult to predict the stress state in the tin after the intermetallic has formed a continuous layer. However, peaks in the roughness will have a qualitatively similar effect to an expanding inclusion and permit the mismatch strain in the intermetallic to be accommodated by plastic flow in the tin. We would expect to observe two modes of deformation: the short-wavelength roughness would cause a local layer of plasticity near the intermetallic/Sn interface, while the longer wavelength would be expected to induce bulk plastic flow in the entire Sn grain, and induce a compressive stress roughly equal to the yield stress of Sn. More-detailed numerical simulations would be helpful to provide further insight into this process.

This picture of stress generation in Sn and relaxation in the intermetallic differs significantly from existing discussions in the literature. In the early work of Tu,[12–14] the Sn/intermetallic interface was assumed to remain planar and stress was assumed to develop in the Sn as a result of ejection of Sn atoms at the advancing Sn/intermetallic interface. The model assumed that whisker

formation is the only mechanism for absorbing the excess Sn, so that whiskers would form wherever the passivating oxide layer on the Sn surface was damaged. Lee and Lee[11] pointed out the importance of the nonplanar nature of the intermetallic but analyzed its consequences using a purely elastic model. Our experiments show that the expansion of the intermetallic particles is accommodated by plastic flow in the surrounding Sn. Instead of generating a highly localized state of stress near the particles, this process results in a state of biaxial compressive stress in the Sn film equal in magnitude to the yield stress of Sn. This stress drives grain-boundary diffusion in the Sn film, which is ultimately responsible for whisker formation. Whiskers may form, for example, in regions where the grain boundary structure is non columnar.[21] An important consequence of this conclusion is that the stresses in the Sn are not sensitive to the details of the mass exchange accompanying the formation of the intermetallic: continuous generation of intermetallic simply ensures that the stresses in the Sn remain comparable to its yield stress.

## V. CONCLUSIONS

A detailed electron microscopy investigation of the microstructural evolution in vapor-deposited Cu/Sn bimetal layer on $SiO_2$ and epoxy substrates was undertaken. The study confirms the presence of submicron (~100 nm) Cu grains and columnar micron-scale Sn grains, the latter being covered for the most part by an adherent, ~5- to 8-nm tin oxide layer. Over time at room temperature, the Cu and Sn layers react to form an intermetallic, $Cu_6Sn_5$, which continues to grow into the Sn grain. Curvature measurements verify the evolution of a compressive stress in the Sn layer that reaches a plateau corresponding approximately, to the yield stress of Sn. Over time, Sn whiskers evolve from the Sn surface.

Our study revealed the following specific findings:

(1) $Cu_6Sn_5$ forms initially, preferentially at locations where the Sn grain boundaries intersect the Cu/Sn interface. With time, the intermetallic appears to grow along the Sn boundaries fairly rapidly while also thickening laterally.

(2) Simultaneously, $Cu_6Sn_5$ also forms heterogeneously at locations where the Cu grain boundaries meet the Cu/Sn interface, and these grow into the Sn grains while impinging on each other laterally, their size and spacing likely being determined by the Cu grain size.

(3) With time, the intermetallic grows in a columnar manner into the Sn grain, the extent of growth being a maximum at the grain boundaries and a minimum at the center of the Sn grain. The intermetallic/Sn interface is cusped at the microscopic column scale, and the individual columns appear to be polycrystalline as well. Cu transport to the advancing intermetallic/Sn interface likely occurs preferentially along the columnar boundaries as well as the intermetallic grain boundaries within the columns.

(4) Even in the early stages of the reaction to form $Cu_6Sn_5$ (i.e., isolated particles at Sn grain boundaries), dislocations appear to be punched out from the intermetallic/Sn interface, a signature of local plastic relaxation of the misfit stress.

(5) These dislocations appear to rearrange rapidly by glide and climb (dynamic recovery), presumably accelerated by point defect generation as a consequence of the misfit strain in addition to the available thermal vacancies at room temperature (~$0.6T_m$ for Sn).

(6) Those dislocations that continue to reach the Sn surface by glide and climb processes (likely driven by stresses arising from Sn diffusion along the grain boundaries) tend to pile up at the oxide layer and can generate elastic stress at the head of the pileup that may be instrumental in cracking the Sn oxide.

(7) As the intermetallic continues to grow, dislocations continue to be punched out and the population of subgrain boundaries increases dramatically and, in the later stages, reaches the Sn surface. Dislocations constituting the subgrain boundary can themselves serve as sources, and these sources can operate when an appropriate stress is available.

(8) When a subgrain boundary intersects the Sn surface (or, for that matter, the $Cu_6Sn_5$ column at the intermetallic/Sn interface from where the dislocations are generated), it locally reconfigures the interface to generate interfacial energy balance. This has the effect of "pulling" the Sn surface in, by cusping, and can produce a delamination stress on the relatively stiffer Sn oxide layer.

(9) Formation of numerous subgrains within a Sn grain produces local misorientation ranging anywhere from 0.1° to 1–2° depending on the type and spacing of dislocations constituting the subgrain boundary. It is argued that the consequence of such rotations could produce surface (and Sn grain boundary) roughening that may also be instrumental in rupturing the Sn oxide.

(10) Lastly, although attention has been given to the role of dislocation glide and climb in accommodating misfit stresses (and how they can produce a stress at the Sn surface), it is pertinent to note that diffusional creep processes (Coble creep or Nabarro–Herring creep and viscous mechanisms) may also contribute to accommodating these stresses. This study has just not generated experimental evidence for these creep processes.

## ACKNOWLEDGMENTS

This work was supported primarily by the MRSEC Program (Micro- and Nano- Mechanics of Materials; Brown University) of the National Science Foundation

under Award DMR-0520651. We acknowledge Mr. Nitin Jadhav for assistance with the stress measurement experiments and Mr. Ratnesh Gupta for measuring the subgrain misorientation in the Sn grains.

## REFERENCES


1. W.C. Ellis, D.F. Gibbons, and R.C. Treuting: Growth of metal whiskers from the solid, in *Growth and Perfection of Crystals*, edited by R.H. Doremus, B.W. Roberts, and D. Turnbull (John Wiley, New York, 1958), pp. 102–120.
2. S.C. Britton: Spontaneous growth of whiskers on tin coatings: 20 years of observation. *Trans. Inst. Met. Finish.* **52,** 95 (1974).
3. R.G. Baker: Spontaneous metallic whisker growth. *Plat. Surf. Finish.* **74**(11), 12 (1987).
4. H.L. Cobb: Cadmium whiskers. *Mon. Rev. Am. Electroplat. Soc.* **33,** 28 (1946).
5. U. Lindborg: Observations on the growth of whisker crystals from zinc electroplate. *Metall. Trans. A* **6,** 1581 (1975).
6. U. Lindborg: A model for the spontaneous growth of zinc, cadmium and tin whiskers. *Acta Metall.* **24,** 181 (1976).
7. F.C. Frank: On tin whiskers. *Philos. Mag.* **44,** 851 (1953).
8. J.D. Eshelby: A tentative theory of metallic whisker growth. *Phys. Rev.* **91,** 755 (1953).
9. M.O. Peach: Mechanism of growth of whiskers on cadmium. *J. Appl. Phys.* **23,** 1401 (1952).
10. S. Amelinckx, W. Bontinck, W. Dekeyser, and F. Seitz: On the formation and properties of helical dislocations. *Philos. Mag.* **2,** 355 (1957).
11. B.Z. Lee and D.N. Lee: Spontaneous growth mechanism of tin whiskers. *Acta Metall.* **46,** 3701 (1998).
12. K.N. Tu: Interdiffusion and reaction in bimetallic Cu–Sn thin films. *Acta Metall.* **21,** 347 (1973).
13. K.N. Tu and R.D. Thompson: Kinetics of interfacial reaction in bimetallic Cu-Sn thin films. *Acta Metall.* **30,** 947 (1982).
14. K.N. Tu: Irreversible processes of spontaneous whisker growth in bimetallic Cu–Sn thin film reactions. *Phys. Rev. B* **49,** 2030 (1994).
15. K.N. Tu: Cu/Sn interfacial reactions: Thin-film case versus bulk case. *Mater. Chem. Phys.* **46,** 217 (1996).
16. B.D. Nordwall: Air Force links radar problems to growth of tin. Whiskers. *Aviation Week Space Technol.* **June 30,** 65 (1986).
17. B. Felps: Whiskers caused satellite failure: Galaxy IV outage blamed on interstellar phenomenon. *Wireless Week* **May 17** (1999).
18. J. Richardson and B. Lasley: Tin whisker initiated vacuum metal arcing in spacecraft electronics, in *Proc. 1992 Government Microcircuit Applications Conference* (GOMAC-92, Las Vegas, NV, November 10–12, 1992), Vol. XVIII, pp. 119–122.
19. L. Corbid: Constraints on the use of tin plate in miniature electronic packages, in *Proc. 3rd International SAMPE Electronics Conference* (Los Angeles, CA, June 20–22, 1989), pp. 773–779.
20. S. Silverstein: Reasons for failure lost with Galaxy 4. *Space News* **Aug. 17–23,** 19 (1998).
21. W.J. Boettinger, C.E. Johnson, L.A. Bendersky, K-W. Moon, M.E. Williams, and G.R. Stafford: Whisker and Hillock formation on Sn, Sn–Cu and Sn–Pb electrodeposits. *Acta Mater.* **53,** 5033 (2005).
22. V.K. Glazunova: A Study of the influence of certain factors on the growth of filamentary tin crystals. *Kristallografiya* **7**(5), 761 (1962).
23. B.D. Dunn: A laboratory study of tin whisker growth. European Space Agency (ESA) Report STR-223 (ESA, Paris, France, 1987), pp. 1–50.
24. K. Tsuji: Role of grain boundary free energy and surface free energy for tin whisker growth, in *Proc. of the IPC/JEDEC 4th Intl. Conf. on Lead-Free Electronic Components and Assemblies* (Frankfurt, Germany, October 21–22, 2003), pp. 169–186.
25. I. Boguslavsky and P. Bush: Recrystallization principles applied to whisker growth in tin, in *Proc. 2003 APEX Conf.* (Anaheim, CA, 2003), pp. S12-4-1–S12-4-10.
26. M.W. Barsoum, E.N. Hoffman, R.D. Doherty, S. Gupta, and A. Zavaliangos: Driving force and mechanism for spontaneous metal whisker formation. *Phys. Rev. Lett.* **93,** 206104-1 (2004).
27. C. Xu, Y. Zhang, C. Fan, and J.A. Abys: Driving force for the formation of Sn whiskers: Compressive stress—Pathways for its generation and remedies for its elimination and minimization. *IEEE Trans. Electron. Packaging Manuf.* **28,** 31 (2005).
28. C. Xu, Y. Zhang, C. Fan, and J. Abys: Understanding whisker phenomenon: The driving force for whisker formation. *CircuiTree Mag.* 94 (2002).
29. W. Zhang, A. Egli, F. Schwager, and N. Brown: Investigation of Sn–Cu intermetallic compounds by AFM: New aspects of the role of intermetallic compounds in whisker formation. *IEEE Trans. Electron. Packaging Manuf.* **28,** 85 (2005).
30. W.J. Choi, T.Y. Lee, K.N. Tu, N. Tamura, R.S. Celestre, A.A. MacDowell, Y.Y. Bong, and L. Nguyen: Tin whiskers studied by synchrotron radiation scanning x-ray micro-diffraction. *Acta Mater.* **51,** 6253 (2003).
31. C. Xu, Y. Zhang, C. Fan, J. Abys, L. Hopkins, and F. Stevie: Understanding whisker phenomenon, driving force for the whisker formation, in *Proc. IPC SMEMA Council APEX 2002* (New Orleans, LA, November 3–7, 2002), pp. S06-2-1–S06-2-6.
32. G.T.T. Sheng, C.F. Hu, W.J. Choi, K.N. Tu, Y.Y. Bong, and L. Nguyen: Tin whiskers studied by focused ion beam imaging and transmission electron microscopy. *J. Appl. Phys.* **92,** 64 (2002).
33. R.M. Fisher, L.S. Darken, and K.G. Carroll: Accelerated growth of tin whiskers. *Acta Metall.* **2,** 368 (1954).
34. R.R. Hasiguti: A tentative explanation of the accelerated growth of tin whiskers. *Acta Metall.* **3,** 200 (1955).
35. M.E. Williams, C.E. Johnson, K.W. Moon, G.R. Stafford, C.A. Handwerker, and W.J. Boettinger: Whisker formation on electroplated SnCu, in *Proc. AESF SUR/FIN Conf.* (Chicago, IL, 2002), pp. 31–39.
36. K.N. Tu and K. Zeng: Reliability issues of Pb-free solder joints in electronic packaging technology, in *Proc. 52nd IEEE Electron. Comp. & Tech. Conf.* (San Diego, CA, May 28–31, 2002), pp. 1194–1199.
37. J. Chang-Bing Lee, Y-L. Yao, F-Y. Chiang, P.J. Zheng, C.C. Liao, and Y.S. Chou: Characterization study of lead-free SnCu plated packages, in *Proc. IEEE Electron. Comp. & Tech. Conf.* (San Diego, CA, May 28–31, 2002), pp. 1238–1245.
38. Y. Zhang, C. Xu, C. Fan, J. Abys, and A. Vysotskaya: Understanding whisker phenomenon, whisker index and tin/copper, tin/nickel interface, in *Proc. IPC SMEMA Council APEX 2002* (New Orleans, LA, November 3–7, 2002), pp. S06-1-1–S06-1-10.
39. Y. Zhang, C. Fan, C. Xu, O. Khaselev, and J.A. Abys: Tin whisker growth-substrate effect: Understanding CTE mismatch and IMC formation. Paper presented at IPC Printed Circuits Expo, SMEMA Council APEX Designers Summit (February 24–26, 2004).
40. G.T. Galyon and L. Palmer: An integrated theory of whisker formation: The physical metallurgy of whisker formation and the role of internal stresses. *IEEE Trans. Elect. Packaging Manuf.* **28,** 17 (2005).
41. J.D. Eshelby: The elastic field outside an ellipsoidal inclusion. *Proc. R. Soc. London A* **252,** 561 (1959).
42. E. Chason and J.A. Floro: Measurements of stress evolution during thin film growth, in *Materials Reliability in Microelectronics*

*VI*, edited by W.F. Filter, J.J. Clement, A.S. Oates, R. Rosenberg, and P.M. Lenahan (Mater. Res. Symp. Proc. **428,** Pittsburgh, PA, 1996), p. 499.

43. J.A. Floro and E. Chason: Curvature based techniques for real-time stress measurements during thin film growth, in *In-Situ Characterization of Thin Film Growth Processes*, edited by A. Krauss and O. Auciello (John Wiley, New York, 2000), p. 191.
44. E. Smith and J. Nutting: Direct carbon replicas from metal surfaces. *Br. J. Appl. Phys.* **7,** 214 (1956).
45. J. Mayer, L.A. Giannuzzi, T. Kamino, and J. Michael: TEM sample preparation and FIB-induced damage. *MRS Bull.* **32**(5), 400 (2007).
46. M. Sobeich, U. Welzel, R. Schuster, E.J. Mittemeijer, W. Hugel, A. Seekamp, and V. Muller: The microstructure and state of stress of Sn thin films after post-plating annealing: An explanation for the suppression of whisker formation? in *Proceedings of the 57th Electronic Components and Technology Conference, ECTC '07* (Reno, NV, May 29–June 1, 2007), pp. 192–197.
47. K.S. Kumar and S.A. Brown: Tensile behavior of the $L1_2$ compound $Al_{67}Ti_{25}Cr_8$. *Acta Metall. Mater.* **40,** 1923 (1992).
48. A.W. Mullendore and N.J. Grant: Grain boundary serrations developed during creep, in *Structural Processes in Creep,* Special Report No. 70 (Iron and Steel Institute, London, 1961), pp. 44–55.
49. F.M.J. Thijssen: Effect of strain on microstructural evolution during dynamic recrystallization: Experiments on tin. Report. Utrecht University, The Netherlands (2004).
50. ASM International. Properties and selection: Non-ferrous alloys and special purpose materials, in *Metals Handbook*, 10th ed. (ASM International, 1990), Vol. 2, pp. 517–526.
51. R.J. McCabe and M.E. Fine: Creep of tin, Sb-solution strengthened tin and SbSn-precipitate–strengthened tin. *Metall. Mater. Trans. A* **33,** 1531 (2002).
52. P. Adeva, G. Caruana, O.A. Ruano, and M. Torralba: Microstructure and high temperature mechanical properties of tin. *Mater. Sci. Eng., A* **194,** 17 (1994).
53. F. Lang, H. Tanaka, O. Munegata, T. Taguchi, and T. Narita: The effect of strain rate and temperature on the tensile properties of Sn–3.5Ag solder. *Mater. Charact.* **54,** 223 (2005).
54. Y-H. Pao, S. Badgley, R. Govila, and E. Jih: An experimental and modeling study of thermal cyclic behavior of Sn–Cu and Sn–Pb solder joints, in *Electronic Packaging Materials Science VII,* edited by P. Borgesen, K.F. Jensen, and R.A. Pollak (Mater. Res. Soc. Symp. Proc. **323**, Pittsburgh, PA, 1994), p. 153.